Low pressure chemical vapor deposition of β-Ga_2O_3 thin films: dependence on growth parameters

Zixuan Feng[1], Md Rezaul Karim[1] and Hongping Zhao[1,2,*]

[1]Department of Electrical and Computer Engineering, The Ohio State University, Columbus, Ohio 43210, USA

[2]Department of Materials Science and Engineering, The Ohio State University, Columbus, Ohio 43210, USA

[*]zhao.2592@osu.edu

Abstract

Low pressure chemical vapor deposition (LPCVD) has been used to produce high quality β-Ga_2O_3 materials with controllable n-type doping. In this work, we focus on the studies of key LPCVD growth parameters for β-Ga_2O_3 thin films, including oxygen/carrier gas flow rates, growth temperature, pressure and the substrate to Ga crucible distance. These growth parameters play important roles during the LPCVD β-Ga_2O_3 growth which determine the thin film growth rate, n-type dopant incorporation, and electron mobilities. The dependence of the growth parameters on LPCVD of β-Ga_2O_3 was carried out on both conventional c-plane sapphire and 6 degree off-axis (toward <11-20> direction) sapphire substrates. To better understand the precursor transport and gas phase reaction process during the LPCVD growth, a numerical model for evaluating the growth rate was developed by using finite element method and taking into account the gas flow rate, chamber pressure and chamber geometry. Results from this work can provide guidance for the optimization of the LPCVD growth of β-Ga_2O_3 with targeted growth rate, surface morphology, doping concentration and mobility. In addition, β-Ga_2O_3 grown on off-axis c-sapphire substrates features with faster growth rates with higher electron mobilities within a wide growth window.

β-Ga_2O_3 with a bandgap of 4.6-4.9 eV, represents an emerging ultrawide bandgap semiconductor, promising for radio frequency and high power device applications. The most stable β phase Ga_2O_3 has a complex monoclinic crystal structure with two Ga sites and three O sites. The large bandgap of β-Ga_2O_3 renders 2-3 times higher critical electric field (6-8 MV/cm) than GaN (3.3 MV/cm) and SiC (2.5 MV/cm) [1-3]. Consequently, β-Ga_2O_3 based power electronic (Baliga's figure of merit, BFoM ~ 3200) and high frequency (Johnson's figure of merit, JFoM ~ 2850) devices show great promises to outperform the existing technologies based on GaN (BFoM ~ 846, JFoM ~ 1090) or SiC (BFoM ~ 317, JFoM ~ 278) [4]. Promising progress has been made for β-Ga_2O_3 based devices. For example, β-Ga_2O_3 enhancement mode metal-oxide-semiconductor field effect transistor (MOSFET) with breakdown voltage > 1kV [5], β-Ga_2O_3 Schottky barrier diode (SBD) with 2.3 kV breakdown voltage [6], and low pressure chemical vapor deposition (LPCVD) β-Ga_2O_3 based vertical SBD with breakdown field of 4.2 MV/cm [7] have been demonstrated recently.

In addition, the large bandgap corresponding to a transition wavelength at ~250 nm enables β-Ga_2O_3 for optoelectronic devices operating in the deep ultraviolet (DUV) wavelength region, e.g., solar blind photodetectors [8]. Another key advantage of β-Ga_2O_3 as compared to the existing wide bandgap semiconductors such as GaN and SiC, is its availability of bulk single crystals synthesized by low cost and scalable melt-based growth methods including floating zone method (FZ) [2, 9-11], Czochralski (CZ) method [12-14] and edge-defined film fed (EFG) method [15, 16]. Currently, the as-synthesized β-Ga_2O_3 substrates exhibit n-type conductivity with doping concentration in the order of 1-9×10^{17} cm^{-3} (N_d-N_a). Both intentionally doped n-type (Sn doped) and semi-insulating (Fe doped) β-Ga_2O_3 substrates are commercially available with different crystal orientations. One challenge associated with β-Ga_2O_3 is its low thermal conductivity which may require thermal management for high power

device applications [4]. The investigation of β-Ga_2O_3 heteroepitaxy on foreign substrate such as sapphire can provide additional flexibility of epi-layer transferring to platforms with higher thermal conductivities.

The growth of β-Ga_2O_3 thin films have been conducted by different growth techniques including molecular beam epitaxy (MBE) [17-24], halide vapor phase epitaxy (HVPE) [25-28], metalorganic chemical vapor deposition (MOCVD) [29-34], LPCVD [8, 35-40], and pulsed laser deposition (PLD) [41, 42]. N-type doping control for β-Ga_2O_3 in the range between 10^{15}-10^{19} cm^{-3} has been achieved [23, 24, 31, 32, 43]. Tin (Sn), germanium (Ge) and silicon (Si) have been investigated as n-type dopants in β-Ga_2O_3 [24, 31, 32]. Room temperature electron mobility of 150 $cm^2/V{\cdot}s$ and 130 $cm^2/V{\cdot}s$ were achieved in MBE and MOCVD grown films, respectively [23, 29].

LPCVD has been demonstrated as a feasible growth method to produce high quality β-Ga_2O_3 thin films with Si as a controllable dopant in a wide range between 10^{17}-10^{20} cm^{-3} and growth rate from < 1μm/hr up to 10 μm/hr [7, 8, 36-40]. Room temperature electron mobility of 100-110 $cm^2/V{\cdot}s$ have been achieved in LPCVD grown homoepitaxial and heteroepitaxial β-Ga_2O_3 films [36, 38, 40]. Using off-axis sapphire substrates, the as-grown LPCVD β-Ga_2O_3 films have shown significantly improved crystalline quality and electron mobility [40]. It was observed that the properties of LPCVD grown β-Ga_2O_3 films highly depend on the growth parameters including the substrate surface preparation, growth temperature, pressure, oxygen flow rate, carrier gas flow rate, and the distance between the substrate and Ga crucible. However, a systematic study of the LPCVD growth conditions on β-Ga_2O_3 is still lacking.

In this work, we have performed a systematic study on the effects of various LPCVD growth parameters on the growth rate, dopant incorporation and carrier mobility in LPCVD β-Ga_2O_3 grown on c-plane sapphire substrates with 0° and 6° off-axis (towards <11-20> direction)

angles. Numerical simulation based on finite element method was used to simulate the vapor transport process and gas phase reaction in the LPCVD growth system.

Si-doped heteroepitaxial β-Ga_2O_3 films were grown on both the conventional and off-axis (Δ_a = 6°) sapphire substrates co-loaded in a custom-built horizontal flow LPCVD system. The system has a precise control of the temperature, gas flow rate, and pressure. High purity metallic gallium (Ga, 99.99999%) and research grade oxygen (O_2, 99.999%) were used as the precursors whereas argon (Ar, 99.9999%) was used as the carrier gas. $SiCl_4$ (3%, balanced with Ar) was used as the n-type dopant source. The metallic Ga source was placed in a crucible inside the growth chamber and the substrates were placed horizontally at the downstream. Prior to growth, the substrates were cleaned by organic solvent in the sequence of acetone, IPA; then sonicated in DI water and finally blow dry by compressed nitrogen. The room temperature doping concentration and carrier mobility of the as-grown samples were characterized by van der Pauw Hall measurement (HMS 3000 Hall measurement system). The 3D computational fluid dynamics were simulated to extract the gas flow velocity by using the COMSOL multi-physics software. The 2D finite element method was used to numerically determine the concentration of gas species and its gradient, for growth rate estimations.

In order to investigate the effects of Ar and O_2 flow rates on the growth of β-Ga_2O_3 films, two series of growth experiments were performed with fixed Ar flow rate of 200 sccm and 300 sccm, respectively. For Ar flow rate of 200 sccm, the O_2 flow rate increases from 5 to 20 sccm; and for Ar flow rate of 300 sccm, the O_2 flow rate increases from 15 to 40 sccm. The growth temperature was kept at 900 ℃, growth time was 30 mins, and $SiCl_4$ flow rate was set as 0.15 sccm. Figures 1 and 2 present the effects of O_2 flow rate on the growth rate, carrier concentration and electron Hall mobility of the as-grown β-Ga_2O_3 films on c-plane sapphire substrates with Δ_a = 0° and 6° for Ar flow rate of 200 and 300 sccm, respectively. As shown in

Figs. 1(a) and 2(a), with fixed Ar flow rate, the growth rate of the films increases with increase of the O_2 flow rate, which suggests that under the investigated growth conditions the growth rate was limited by the O_2 flow rate. The films grown on off-axis substrates show faster growth rates than those on the conventional c-plane sapphire substrates with the identical growth conditions. The terrace surface morphology of the off-axis substrates provides preferred incorporation sites for the adatoms which facilitate faster growth rates [40].

The electron concentration in both cases shows a decrease trend as the O_2 flow rate increases as shown in Figs. 1(b) and 2(b). This can result from the faster growth rates as the O_2 flow rate increases. In LPCVD, the incorporation rate of dopant atoms per unit volume (N_D) can be predicted from the following equation [44]:

$$N_{\mathrm{D}} = J_{\mathrm{D}} S_{\mathrm{D}} \frac{1}{G_r} \tag{1}$$

where J_D represents the dopant flux to the growth surface, S_D is the sticking coefficient and G_r is the growth rate. N_D is inversely proportional to the growth rate G_r, and our experiments show a consistent trend as predicted by equation (1). The Si dopant incorporation efficiency is similar for β-Ga_2O_3 films grown on both conventional and off-axis sapphire substrates. With the Ar flow rate of 200 sccm, as shown in Fig. 1(c), the corresponding electron Hall mobility increases as O_2 flow rate increases. This can be related to the reduced carrier concentration with the increase of O_2 flow rate. The electron mobility of the film grown on off-axis sapphire substrate shows enhanced mobilities within the growth conditions investigated. The extended defects originating from the sapphire/Ga_2O_3 interface tend to tilt and terminate within the 1-2 μm film thickness, which leads to improved crystalline quality and electron mobility [40]. On the other hand, with Ar flow rate of 300 sccm, the electron mobilities show a different trend. The electron mobility reaches peak at the O_2 flow rate of 30 sccm. Note that the limiting factors for electron mobility of β-Ga_2O_3 films grown on sapphire substrates are more complicated than those

grown on native substrates due to the existence of dislocations from the lattice mismatch. The trend indicates that the electron mobilities are not only limited by impurity scattering, but also other factors such as dislocations and native defects. And the β-Ga_2O_3 films grown on the off-axis sapphire substrates still show enhanced mobilities under the investigated growth conditions.

The growth temperature typically plays an important role for any semiconductor material. In this study, we investigated the effects of the growth temperature on the LPCVD growth of β-Ga_2O_3 thin films. The growth temperature is measured by the thermocouple placed at the center of the furnace. A series of samples were grown at different temperatures ranging between 820 ℃ and 940 ℃ on c-plane sapphire substrates ($\Delta_a = 0°$ and $\Delta_a = 6°$). Ar/O_2 flow rate of 300/30 sccm was used for all the samples with a fixed dopant flow rate of 0.15 sccm. As shown in Fig. 3(a), the growth rate increases monotonically as the increase of growth temperature. During the LPCVD growth of β-Ga_2O_3, the metallic Ga evaporation rate increases as the temperature increases, and therefore, the available Ga vapor transported to the substrate surface increases as the temperature increases. Overall, the growth rate for β-Ga_2O_3 on off-axis sapphire substrate is higher than that of the conventional substrate for all the investigated temperatures. However, when the growth temperature is above 900 ℃, the growth rate on off-axis sapphire substrate shows saturation. At high growth temperatures, it is reasonable to assume that the growth is mass-transport limited [45]. Factors such as gas phase reaction, desorption of adatoms from the substrate surface and decomposition of Ga_2O_3 are expected to play more important roles at elevated temperatures [46], which can lead to the saturation of the growth rate.

The carrier concentration shows a monotonically decrease as the growth temperature increases as shown in Fig. 3(b). This is believed to be mainly due to the reduced dopant

incorporation as the growth rate increases as predicted in Eq. (1) [44]. Additionally, growth condition such as growth temperature and chamber pressure can also affect the diffusion of precursor species in the gas phase, surface adhesion and desorption process. The electron mobilities of β-Ga_2O_3 films grown on off-axis sapphire substrates are higher than those grown on the conventional sapphire, mainly due to the better crystalline quality. The electron mobility of the films grown on off-axis sapphire increases as the temperature increases to 920 ℃ but decreases as the growth temperature increases further. Note that as the temperature increases, Ga evaporation rate increases. Meanwhile, the growth temperature also affects the gas phase reaction between Ga and O. Therefore, with fixed Ar and O_2 flow rate, the atomic ratio of Ga and O on the substrate varies as a function of the growth temperature. As the growth temperature increases to 920 ˚C, the decrease of the electron mobility can be related to the increase of native defects such as vacancies. On the other hand, the mobility of the films grown on the conventional sapphire shows a weak dependence on the growth temperature. This is mainly due to the existence of high density of dislocations in the β-Ga_2O_3 films which limits the electron mobility. Tuning of the growth temperature does not effectively reduce the dislocation density. The electron mobility of β-Ga_2O_3 films shows weak dependence on the carrier concentration. On the other hand, for the films grown on off-axis sapphire substrates, the electron mobilities have a stronger dependence on the carrier concentration, which indicates the films have better crystalline quality.

From our studies, the growth pressure also plays an important role for the LPCVD growth of β-Ga_2O_3. In this study, we performed a controlled growth with the variation of the chamber pressure at 1.7, 3.2, 5.8, 8.8 and 11.1 Torr on c-plane sapphire substrates (Δ_a = 0° and 6°). The growth temperature was set at 900 ℃ and the Ar/O_2 flow rate was kept at 200/15 sccm. As shown in Fig. 4 (a), the film growth rate decreases rapidly with the increase in pressure for both types of substrates, which can be due to the dominant gas phase reaction at higher growth

pressure conditions [47]. Note that at the same pressure, the growth rate difference between the two types of substrates are more obvious, which indicates that growth pressure dependence on off-axis substrates is more sensitive to the growth pressure. For the films grown on the off-axis sapphire substrates, the doping concentration increases as the chamber pressure increases and reaches the peak value at 8.8 Torr (Fig. 4(b)). On the other hand, for the case of $\Delta_a = 0°$, the measured carrier concentration increases with increase in chamber pressure up to 8.8 Torr. However, no continuous films were obtained at pressure of 11.1 Torr and above. Therefore, carrier concentrations in these films were not included here. This can be due to the suppressed surface diffusivity of the adatoms under higher pressures. The flux of dopant species delivered to the growth surface can be determined from the basic diffusion equation:

$$J_D = -D_D \frac{\partial C_D}{\partial y} \tag{2}$$

where D_D is the diffusivity of the dopant species in the chamber, and $\partial C_D/\partial y$ is the concentration gradient of the dopant species above the growth surface (y-axis is perpendicular to the surface). The dependence of the pressure on the LPCVD growth of β-Ga_2O_3 thin films can be resulted from the effects of both parameters: diffusivity and concentration gradient at different pressure. On the other hand, for films grown on both $\Delta_a = 0°$ and 6° sapphire substrates, the electron mobility reaches maximum at relatively low pressures below 3.2 Torr (Fig. 4(c)). Note that the doping incorporation for the materials grown on the two types of substrates are very similar (Fig. 4(b)) despite their different growth rates (Fig. 4(a)). From Fig. 1(b), Fig. 2(b), Fig. 3(b) and Fig. 4(b), we observe that, with the same growth condition, the carrier concentration on both types of substrates are similar. This is due to their similar adatom ratio of Si and Ga on both substrates at the same growth condition.

In addition to the parameters of the gas flow rate, growth temperature and growth pressure, the distance between the substrate and the Ga crucible also plays a critical role in the

LPCVD β-Ga_2O_3 film growth. A series of growths were performed on the off-axis sapphire substrates with controlled pressure at 1.7, 5.4, 11.3 and 15.6 Torr. For each pressure, four samples were placed at horizontally different locations with respect to the Ga crucible. The growth temperature was set at 900 ℃ and the gas flow rate of Ar/O_2 was set as 200/15 sccm. Figure 5 plots the dependence of growth rate *G* as a function of the source to substrate distance *x* at different pressure. The general trend shows that the film growth rate decreases exponentially as the source to substrate distance *x* increases, which is mainly due to the precursor gas phase reactions. To better understand this phenomenon, we conducted a numerical simulation assuming the growth condition to be Ga rich. The growth rate is then primarily determined by the O_2 flux to the growth surface.

For the LPCVD setup as shown in Fig. 6, the second order Fick's law was used [48]:

$$\frac{\partial C(x,y)}{\partial t} = D\left\{\frac{\partial^2 C(x,y)}{\partial x^2} + \frac{\partial^2 C(x,y)}{\partial y^2}\right\} - \bar{v}\frac{\partial C(x,y)}{\partial x} - kC = 0 \quad (3)$$

where *C*, *D* and $\bar{v}$ represent the mass concentration, the gas phase diffusivity of O_2, and the average velocity of O_2 in the chamber, respectively. *k* is the gas phase reaction rate of oxygen. On the other hand, the diffusion flux (*J*) to the substrate surface can be written as:

$$J(x) = -D\frac{\partial C(x,y)}{\partial y}\Big|_{y=0} \quad (4)$$

Considering Eq. 3 and Eq. 4 and assuming that all the oxygen that reaches the substrate surface, or the reactor wall is consumed or deposited, and the radial concentration gradient at the center of the chamber to be zero, the growth rate as a function of *x* can be written as [48]:

$$G(\mathrm{x}) = \frac{M_{Ga_2O_3}}{\rho_{film} M_{O_2}} J(x) = \frac{2M_{Ga_2O_3}}{\rho_{film} M_{O_2}} \frac{C_0 D}{d} e^{-\frac{\pi^2 Dx}{4\bar{v}d^2}} e^{-\frac{kx}{\bar{v}}} \quad (5)$$

where ρ_{film} is the volume mass density of β-Ga_2O_3, C_0 is the density of oxygen at the location of the Ga source, M represents the molecular weight of the species. To fit the calculated growth rate from Eq. 5 over the experimental data as shown in Fig. 5, the values of C_0, $\bar{v}$, D and k are required. Among these parameters, concentration C_0 can be estimated from the ideal gas equation and diffusion coefficient D is calculated by the empirical formula expressed by Chapman-Enskog theory [49]. In order to obtain $\bar{v}$, a simulation of the gas flow in the chamber was performed using computational fluid dynamics (CFD). The standard gas flow rate at the inlet and the pressure at the outlet of the growth chamber were used as the boundary conditions in the CFD simulation. Figure 7 (a) shows the gas velocity contour plot inside the chamber. The velocity was found to be inversely proportional to the chamber pressure, as indicated by the ideal gas law [49]:

$$\bar{v} = \frac{F_{\text{mix}}}{C_{\text{mix}}} = \frac{F_{\text{mix}}RT}{M_{\text{mix}}P} \propto \frac{1}{P} \tag{6}$$

where F_{mix} is the mass flux of Ar/O_2 gas mixture; C_{mix} is the concentration; and M_{mix} is the average molar mass of Ar/O_2 mixture.

In Eq. 5, there are two terms have the exponential decay as a function of x. The first term $e^{-\frac{\pi^2 Dx}{4\bar{v}d^2}}$ can be interpreted as the growth rate decay due to the consumption of O_2 species in gas phase through diffusion and deposition of Ga_2O_3 on the substrate. The second term $e^{-\frac{kx}{\bar{v}}}$ represents the consumption of O_2 species due to gas phase reaction. For the diffusion process between two gas species, it is known that the diffusion coefficient is inversely proportional to the gas pressure P [50]. Therefore, the first term $e^{-\frac{\pi^2 Dx}{4\bar{v}d^2}}$ is found to be independent of pressure P. And in the second term $e^{-\frac{kx}{\bar{v}}}$, $-\frac{k}{\bar{v}}$ is proportional to P. With higher growth pressure, the slower gas flow takes longer time to transport oxygen to the substrate, during which more

oxygen is consumed via the gas phase reaction. The following equation can be obtained by including both terms:

$$G(x) \propto e^{\alpha x}, \ \ \alpha = -\frac{\pi^2 D}{4\bar{v}d^2} - \frac{k}{\bar{v}} \tag{7}$$

Using the four sets of experimental data as shown in Fig. 5, the decay rate α for each pressure condition can be extracted. We find that α is proportional to the pressure, which indicates that between the two components in α, the second term $e^{-\frac{kx}{\bar{v}}}$ is dominant. This indicates the severe gas phase reactions during the LPCVD β-Ga_2O_3 epitaxy. By fitting the experimental data, we extracted the first order reaction rate of O_2 k as ~160 s^{-1}. With the extracted reaction rate, the partial differential equation (3) was solved numerically as a function of $\bar{v}$ and C_0 for each chamber pressure, and O_2 flow rate. Based on the gradient of O_2 concentration, we calculated the dependence of growth rate on the O_2 flow rate and chamber pressure, as shown in Fig. 7(b). With a fixed O_2 flow rate in the growth system, the model predicts that 1) at relatively higher pressure (> 2.8 Torr), the growth rate decreases as the pressure increases, due to the strong consumption of O_2 species via the gas phase reaction; and 2) at a relatively lower pressure range (1.8-2.8 Torr), the growth rate decreases as the pressure decreases. Although the gas phase reaction is suppressed at lower pressures, the O_2 concentration is lower and thus limits the growth rate.

In summary, a systematic study was performed to understand the dependence of key growth parameters on LPCVD β-Ga_2O_3 thin films. The results reveal that O_2 flow rate, growth temperature, growth pressure, and the distance between Ga crucible and substrate all play important roles for the LPCVD growth of β-Ga_2O_3, which determine the growth rate, dopant incorporation, and electron mobilities of the as-grown films. The pressure dependence studies demonstrated that gas transport and diffusion process as well as the precursor gas phase

reaction are greatly influenced by the chamber pressure. The studies of the placement of the growth substrates with respect to the Ga crucible revealed an exponential decay of the growth rate along the horizontal chamber, which is mainly due to the precursor gas phase reaction. The use of off-axis sapphire substrates resulted in faster growth rates and higher electron mobilities within a wide LPCVD growth window. The studies and results from this work provide guidance for LPCVD of β-Ga_2O_3 with targeted growth rate, doping concentration and electron mobilities, which are indispensable for device applications.

Acknowledgments

The authors acknowledge the funding support from the National Science Foundation (DMR-1755479).

Reference

1. H. H. Tippins, Phys. Rev. **140**, A316 (1965).

2. N. Ueda, H. Hosono, R. Waseda, and H. Kawazoe, Appl. Phys. Lett. **71**, 933 (1997).

3. J. B. Varley, J. R. Weber, A. Janotti, and C. G. Van de Walle, Appl. Phys. Lett. **97**, 142106 (2010).

4. S. J. Pearton, J. Yang, P. H. Cary, F. Ren, J. Kim, M. J. Tadjer, and M. A. Mastro, Appl. Phys. Rev. **5**, 011301 (2018).

5. Z. Hu, K. Nomoto, W. Li, N. Tanen, K. Sasaki, A. Kuramata, T. Nakamura, D. Jena and H. G. Xing, IEEE Electron Device Lett. **39**, 869 (2018).

6. J. Yang, F. Ren, M. Tadjer, S. J. Pearton, and A. Kuramata, ECS J. Solid State Sci. Technol. **7**, Q92 (2018).

7. C. Joishi, S. Rafique, Z. Xia, L. Han, S. Krishnamoorthy, Y. Zhang, S. Lodha, H. Zhao, and S. Rajan, Appl. Phys. Express **11**, 031101 (2018).

8. S. Rafique, L. Han, and H. Zhao, Phys. Status Solidi A **214**, 1700063 (2017).

9. E. G. Víllora, K. Shimamura, Y. Yoshikawa, K. Aoki, and N. Ichinose, J. Cryst. Growth **270**, 420 (2004).

10. S. Ohira , N. Suzuki, N. Arai, M. Tanaka, T. Sugawara, K. Nakajima, and T. Shishido, Thin Solid Films **516**, 5763 (2008).

11. N. Suzuki, S. Ohira, M. Tanaka, T. Sugawara, K. Nakajima and T. Shishido, Phys. Status Solidi C **4**, 2310 (2007).

12. Z. Galazka, R. Uecker, D. Klimm, K. Irmscher, M. Naumann, M. Pietsch, A. Kwasniewski, R. Bertram, S. Ganschow, and M. Bickermann, ECS J. Solid State Sci. Technol. **6**, Q3007 (2017).

13. Z. Galazka, R. Uecker, K. Irmscher, M. Albrecht, D. Klimm, M. Pietsch, M. Brützam, R. Bertram, S. Ganschow, and R. Fornari, Cryst. Res. Technol. **45**, 1229 (2010).

14. Y. Tomm, P. Reiche, D. Klimm, and T. Fukuda, J. Cryst. Growth **220**, 510 (2000).

15. A. Kuramata, K. Koshi, S. Watanabe, Y. Yamaoka, T. Masui and S. Yamakoshi, Jpn. J. Appl. Phys. **55**, 12 (2016).

16. V. I. Vasyltsiv, Y. I. Rym and Y. M. Zakharko, Phys. Status Solidi B **195**, 653 (1996).

17. K. Sasaki, M. Higashiwaki, A. Kuramata, T. Masui and S. Yamakoshi, J. Cryst. Growth **392**, 30 (2014).

18. T. Oshima, T. Okuno and S. Fujita, Jpn. J. Appl. Phys. **46**, 7127 (2007).

19. K. Sasaki, M. Higashiwaki, A. Kuramata, T. Masui and S. Yamakoshi, J. Cryst. Growth **378,** 591 (2013).

20. H. Okumura, M. Kita, K. Sasaki, A. Kuramata, M. Higashiwaki and J. S. Speck, Appl. Phys. Express **7**, 095501 (2014).

21. T. Oshima, N. Arai, N. Suzuki, S. Ohira and S. Fujita, Thin Solid Films **516**, 5768 (2008).

22. A. S. Pratiyush, S. Krishnamoorthy, S. V. Solanke, Z. Xia, R. Muralidharan, S. Rajan, and D. N. Nath, Appl. Phys. Lett. **110**, 221107 (2017).

23. K. Sasaki, A. Kuramata, T. Masui, E. G. Víllora, K. S. and S. Yamakoshi, Appl. Phys. Express **5**, 035502 (2012).

24. E. Ahmadi, O. S. Koksaldi, S. W. Kaun, Y. Oshima, D. B. Short, U. K. Mishra, and J. S. Speck, Appl. Phys. Express **10**, 041102 (2017).

25. K. Nomura, K. Goto, R. Togashi, H. Murakami, Y. Kumagai, A. Kuramata, S. Yamakoshi and A. Koukitu, J. Cryst. Growth **405**, 19 (2014).

26. Y. Oshima, E.G. Víllora, K. Shimamura, J, Cryst. Growth **410**, 53 (2015).

27. H. Murakami, K. Nomura, K. Goto, K. Sasaki, K. Kawara, Q. T. Thieu, R. Togashi, Y Kumagai, M. Higashiwaki, A. Kuramata, and S. Yamakoshi, Appl. Phys. Express **8**, 015503 (2014).

28. V. I. Nikolaev, A. I. Pechnikov, S. I. Stepanov, I. P. Nikitina, A. N. Smirnov, A.V. Chikiryaka, S. S. Sharofidinov, V. E. Bougrov, A. E. Romanov, Mater. Sci. Semicond. Process. **47**, 16 (2016).

29. M. Baldini, M. Albrecht, A. Fiedler, K. Irmscher, R. Schewski, and G. Wagner, ECS J. Solid State Sci. Technol. **6**, Q3040 (2017).

30. M. Baldini, M. Albrecht, A. Fiedler, K. Irmscher, D. Klimm, R. Schewski, and G. Wagner, J. Mater. Sci. **51**, 3650 (2016).

31. X. Du, Z. Li, C. Luan, W. Wang, M. Wang, X. Feng, H. Xiao, and J. Ma, J. Mater. Sci. **50**, 3252 (2015).

32. M. Baldini, M. Albrecht, D. Gogova, R. Schewski, and G. Wagner, Semicond. Sci. Technol. **30**, 024013 (2015).

33. D. Gogova, G. Wagner, M. Baldini, M. Schmidbauer, K. Irmscher, R. Schewski, Z. Galazka, M. Albrecht, and R. Fornari, J. Cryst. Growth **401,** 665 (2014).

34. F. Alema, B. Hertog, A. Osinsky, P. Mukhopadhyay, M. Toporkov, and W. V. Schoenfeld, J. Cryst. Growth **475**, 77 (2017).

35. S. Rafique, L. Han, H. Zhao, Phys. Status Solidi A **213**, 1002 (2016).

36. S. Rafique, L. Han, A. T. Neal, S. Mou, M. J. Tadjer, R. H. French, and H. Zhao, Appl. Phys. Lett. **109**, 132103 (2016).

37. S. Rafique, L. Han, M. J. Tadjer, J. A. Freitas Jr, N. A. Mahadik, and H. Zhao, Appl. Phys. Lett. **108**, 182105 (2016).

38. S. Rafique, M. R. Karim, J. M. Johnson, J. Hwang, and H. Zhao, Appl. Phys. Lett. **112**, 052104 (2018).

39. S. Rafique, L. Han, S. Mou, and H. Zhao, Opt. Mater. Express **7**, 3561 (2017).

40. S. Rafique, L. Han, A. T. Neal, S. Mou, J. Boeckl, and H. Zhao, Phys. Status Solidi A **215**, 1700467 (2018).

41. A. Petitmangin, B. Gallas, C. Hebert, J. Perriere, L. Binet, P. Barboux, and X. Portier, Appl. Surf. Sci. **278**, 153 (2013).

42. M. Orita, H. Hiramatsu, H. Ohta, M. Hirano, and H. Hosono, Thin Solid Films **411**, 134 (2002).

43. M. Higashiwaki, K. Sasaki, H. Murakami, Y. Kumagai, A. Koukitu, A. Kuramata, T. Masui, and S. Yamakoshi, Semicond. Sci. Technol. **31,** 034001 (2016).

44. P. Kisliuk, J. Phys. Chem. Solids **3**, 95 (1957).

45. D. L. Smith, *Thin-film deposition: principles and practice*, (McGraw-Hill, Inc., New York, 1995) p. 357.

46. P. Vogt and O. Bierwagen, Appl. Phys. Lett. **108**, 072101 (2016)

47. S. De Persis, A. Dollet, and F. Teyssandier, J. Chem. Educ. **81**, 832 (2004).

48. P. C. Rundle, Int. J. Electronics, **24**, 405 (1968).

49. M. Ohring, *Materials Science of Thin Films: Deposition and Structure (2nd ed.)*, (Academic Press, San Diego, 2002) p.295.

50. E. L. Cussler, *Diffusion: Mass Transfer in Fluid Systems (2nd ed.)*, (Cambridge University Press, New York, 1997) p. 119.

Figures Captions

Figure 1. The dependence of LPCVD n-type β-Ga_2O_3 thin film (a) growth rate, (b) carrier concentration, and (c) electron Hall mobility on O_2 flow rate, with a constant Ar flow rate of 200 sccm. The $SiCl_4$ flow rate was fixed at 0.15 sccm. All samples were grown at 900 ℃ for 30 minutes.

Figure 2. The dependence of LPCVD n-type β-Ga_2O_3 thin film (a) growth rate, (b) carrier concentration, and (c) electron Hall mobility on O_2 flow rate, with a constant Ar flow rate of 300 sccm. The $SiCl_4$ flow rate was fixed at 0.15 sccm. All samples were grown at 900 ℃ for 30 minutes.

Figure 3. The dependence of LPCVD n-type β-Ga_2O_3 thin film (a) growth rate, (b) carrier concentration, and (c) electron Hall mobility on growth temperature. The Ar/O_2 flow rate ratio was fixed at 300/30 and $SiCl_4$ flow rate was fixed at 0.15 sccm. All samples were grown for 30 minutes.

Figure 4. The dependence of LPCVD n-type β-Ga_2O_3 thin film (a) growth rate, (b) carrier concentration, and (c) electron carrier Hall mobility in LPCVD grown β-Ga_2O_3 thin films on chamber pressure. The samples were grown at 900 °C for 30 minutes with Ar/O_2 flow rate ratio of 200/15 and $SiCl_4$ flow rate of 0.15 sccm.

Figure 5. The growth rate (G_r) of LPCVD β-Ga_2O_3 thin films vs. the distance (x) between the Ga source and substrate with different chamber pressures. All samples were grown at 900 ℃ with 200 sccm Ar and 15 sccm O_2 flow rates.

Figure 6. The schematic of horizontal LPCVD chamber illustrating the position of the metallic source, the substrate, and the gas flow direction as marked by arrow. The boundary conditions used in the gas transport modeling are indicated.

Figure 7. (a) The velocity contour of mixed gas flowing in the chamber during growth, obtained from 3-D CFD simulation. The Ar/O_2 flow rate ratio was set as 200/15 at the upstream

of the tube. The Chamber pressure at the downstream was set as 5.4 Torr. (b) The simulated β-Ga_2O_3 thin film growth rate as a function of the oxygen flow rate and chamber pressure. The Argon flow rate was fixed at 300 sccm. The distance between the substrate and Ga precursor was kept at 5 cm.

Figure 1

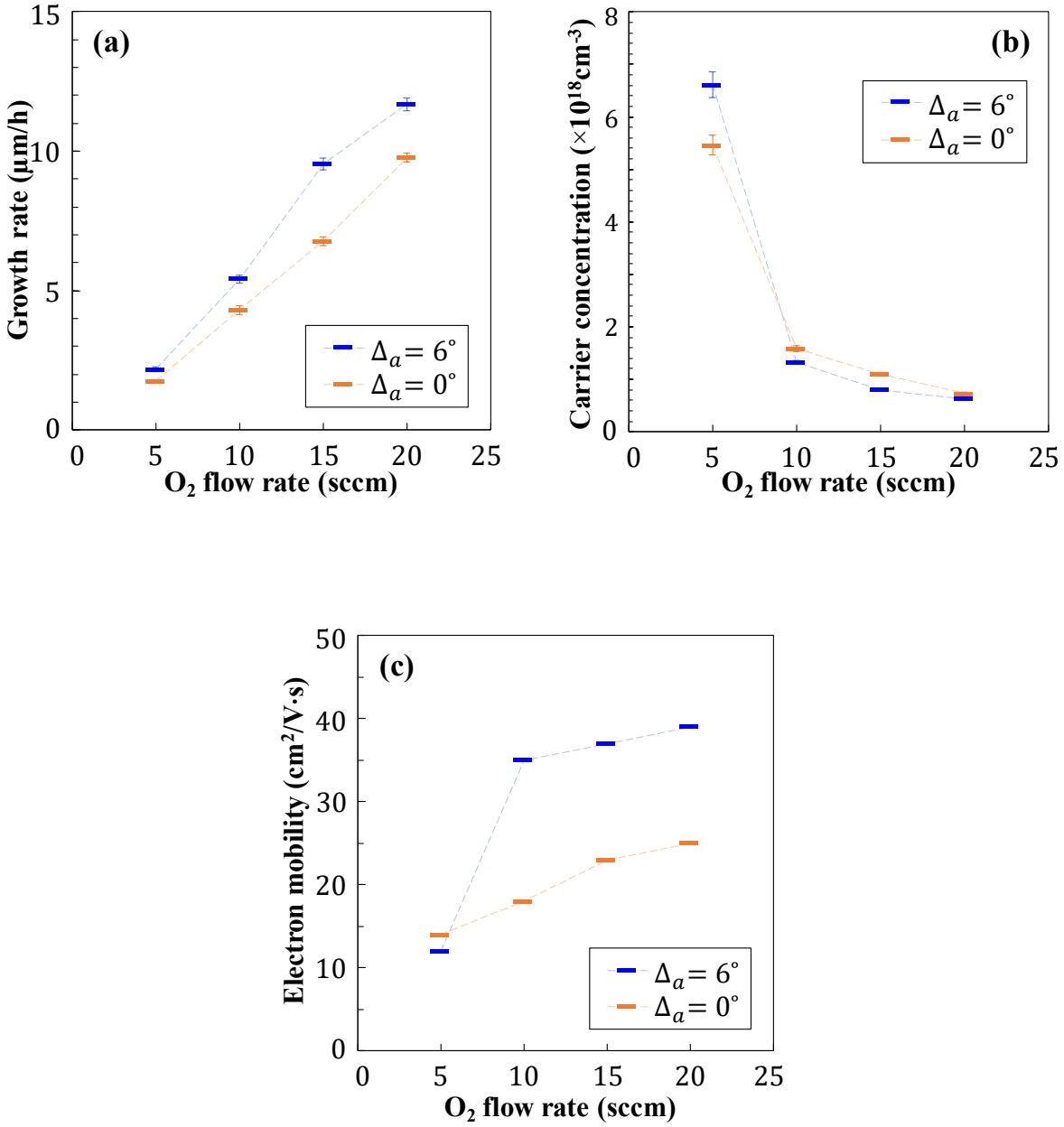
(a)
Growth rate (μm/h)
O2 flow rate (sccm)
Δa = 6°
Δa = 0°
(b)
Carrier concentration (×10^18 cm^-3)
O2 flow rate (sccm)
Δa = 6°
Δa = 0°
(c)
Electron mobility (cm^2/V·s)
O2 flow rate (sccm)
Δa = 6°
Δa = 0°

Figure 2

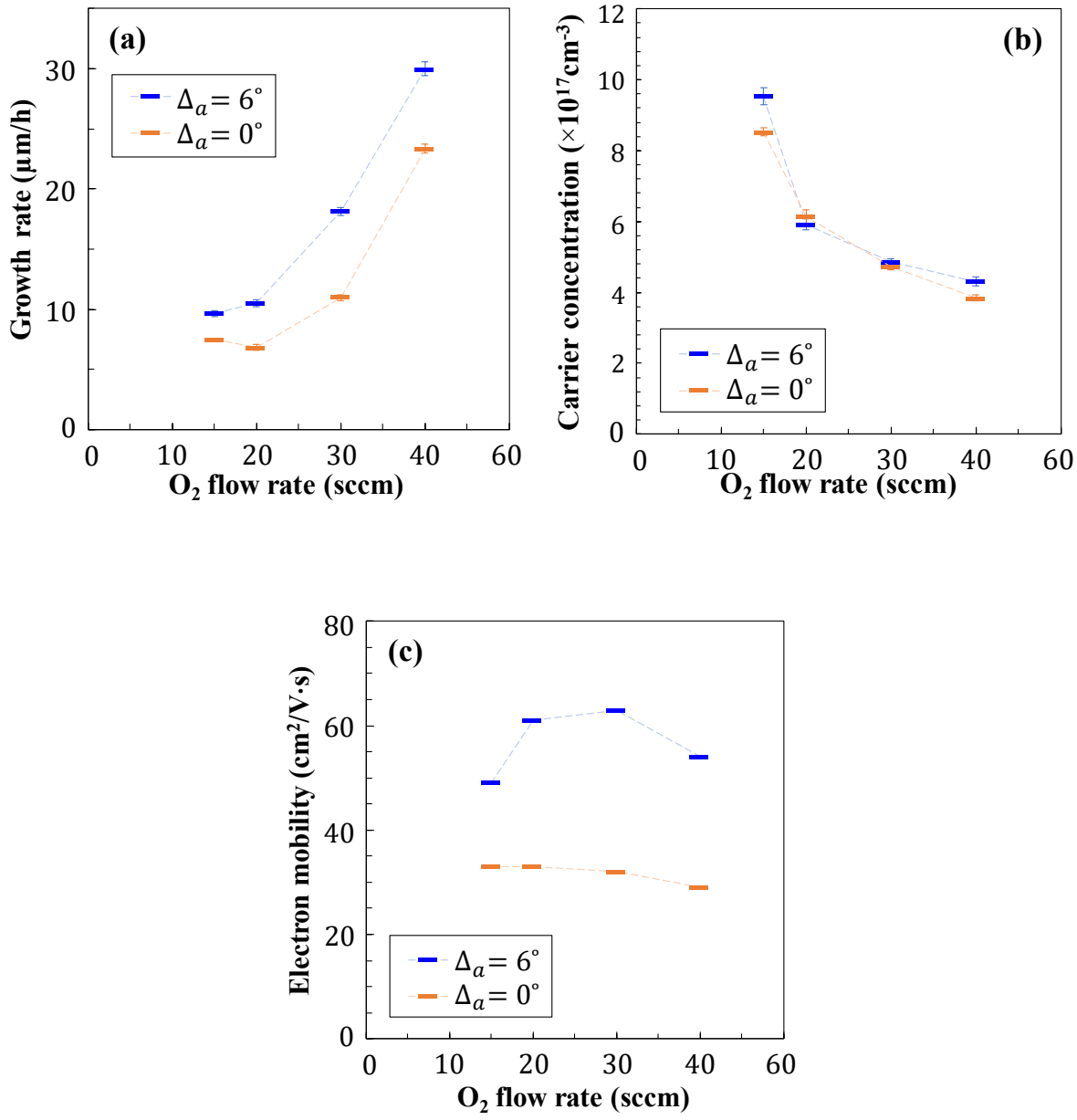
(a)
Growth rate (μm/h)
O2 flow rate (sccm)
Δa = 6°
Δa = 0°
(b)
Carrier concentration (×10^17cm^-3)
O2 flow rate (sccm)
Δa = 6°
Δa = 0°
(c)
Electron mobility (cm^2/V·s)
O2 flow rate (sccm)
Δa = 6°
Δa = 0°

Figure 3

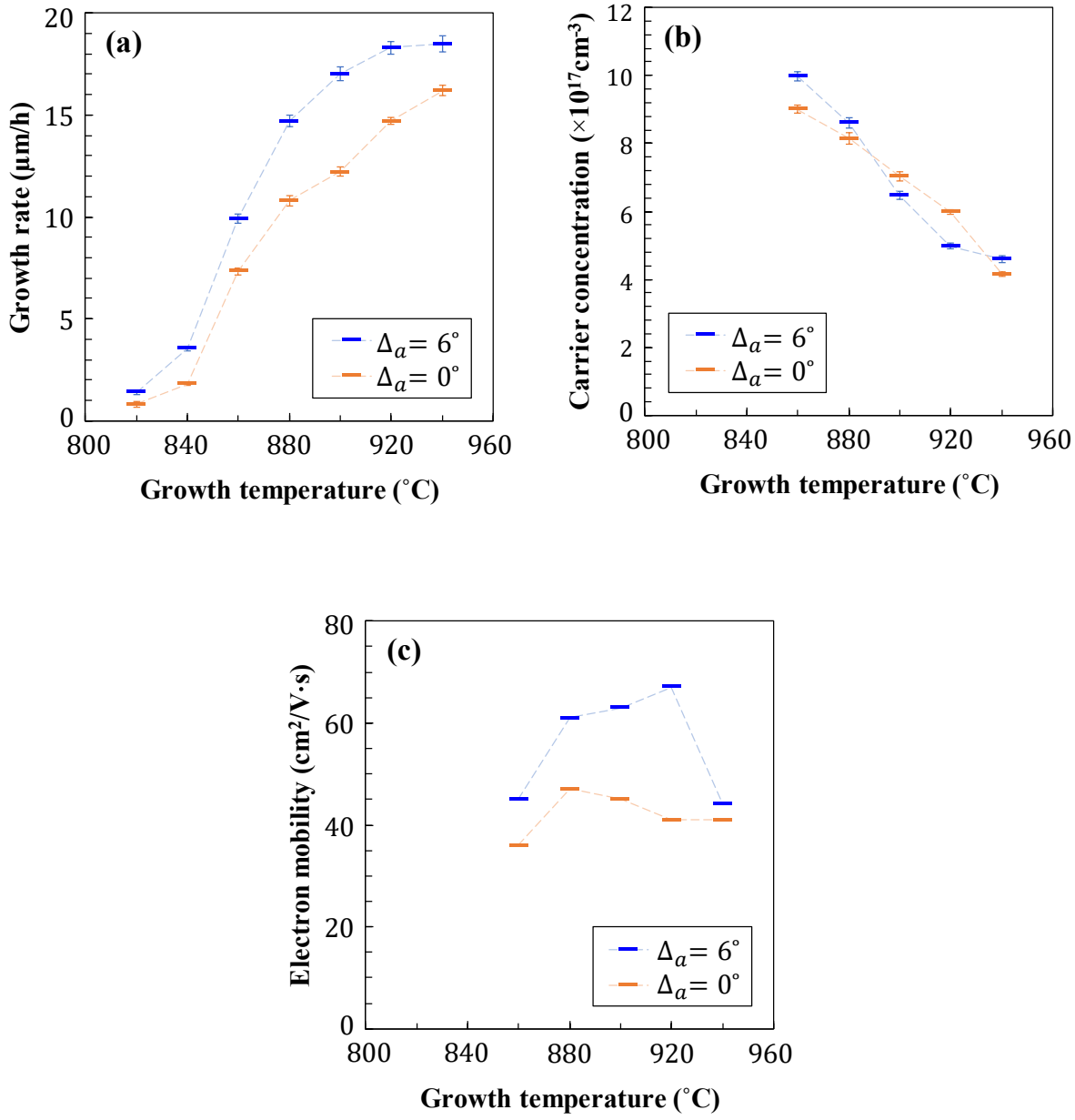
(a)
Growth rate (μm/h)
Growth temperature (˚C)
Δa= 6°
Δa= 0°
(b)
Carrier concentration (×10^17cm^-3)
Growth temperature (˚C)
Δa= 6°
Δa= 0°
(c)
Electron mobility (cm²/V·s)
Growth temperature (˚C)
Δa= 6°
Δa= 0°

Figure 4

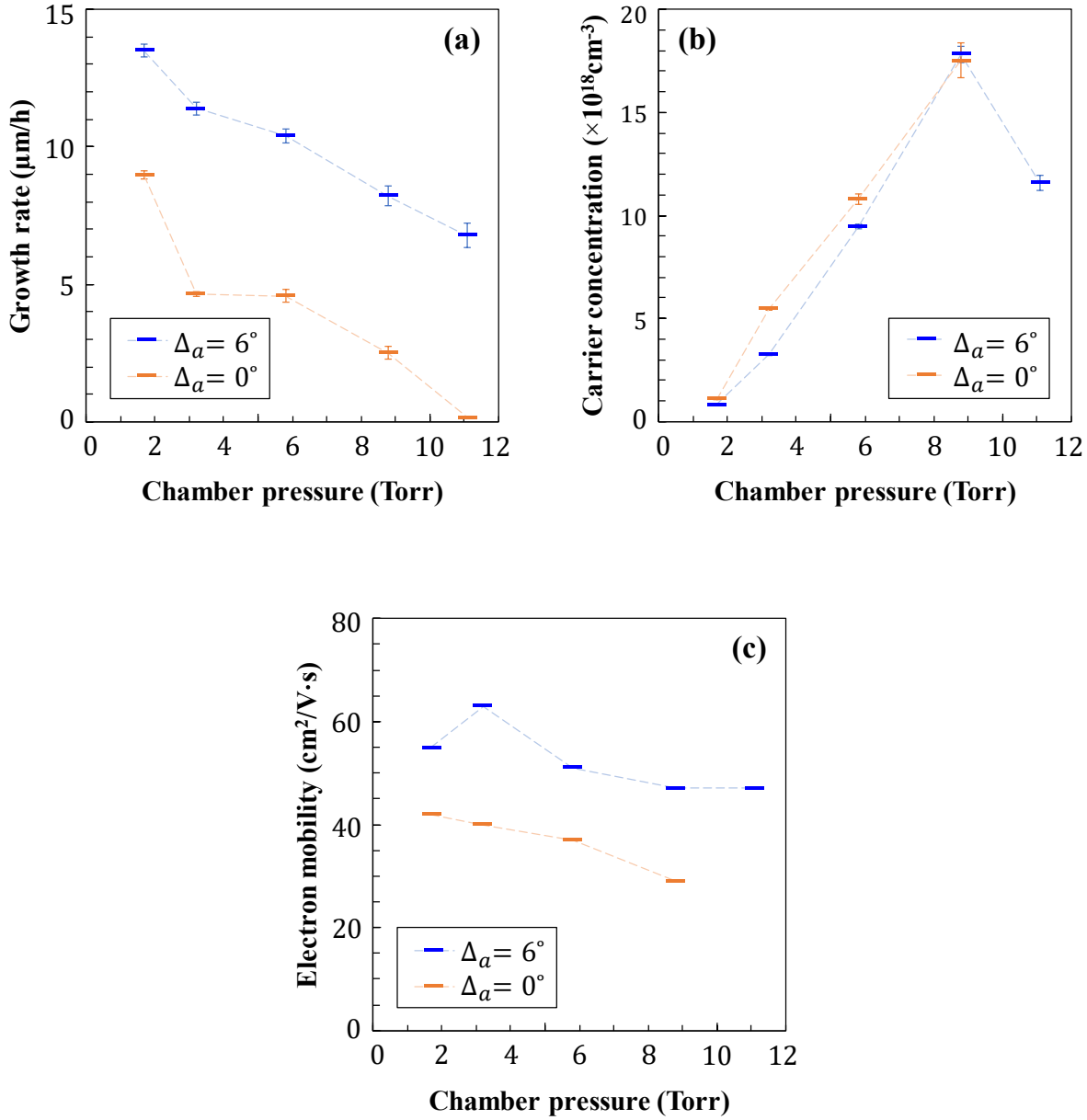
(a)
Growth rate (μm/h)
Chamber pressure (Torr)
Δa= 6°
Δa= 0°
(b)
Carrier concentration (×10^18cm^-3)
Chamber pressure (Torr)
Δa= 6°
Δa= 0°
(c)
Electron mobility (cm²/V·s)
Chamber pressure (Torr)
Δa= 6°
Δa= 0°

Figure 5

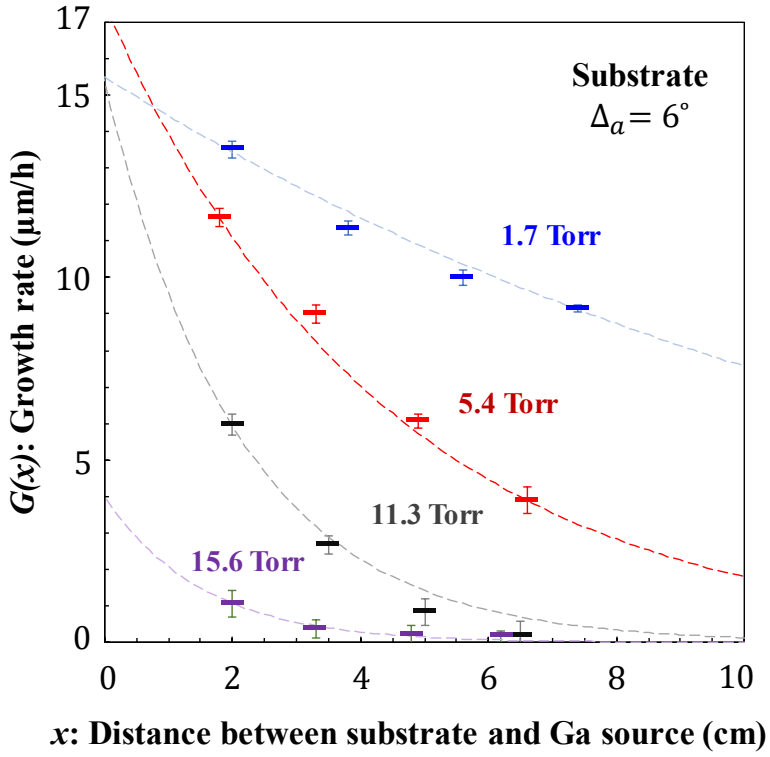
Substrate
$\Delta_a = 6^\circ$
1.7 Torr
5.4 Torr
11.3 Torr
15.6 Torr
G(x): Growth rate (μm/h)
x: Distance between substrate and Ga source (cm)
0
5
10
15
17
0
2
4
6
8
10

Figure 6

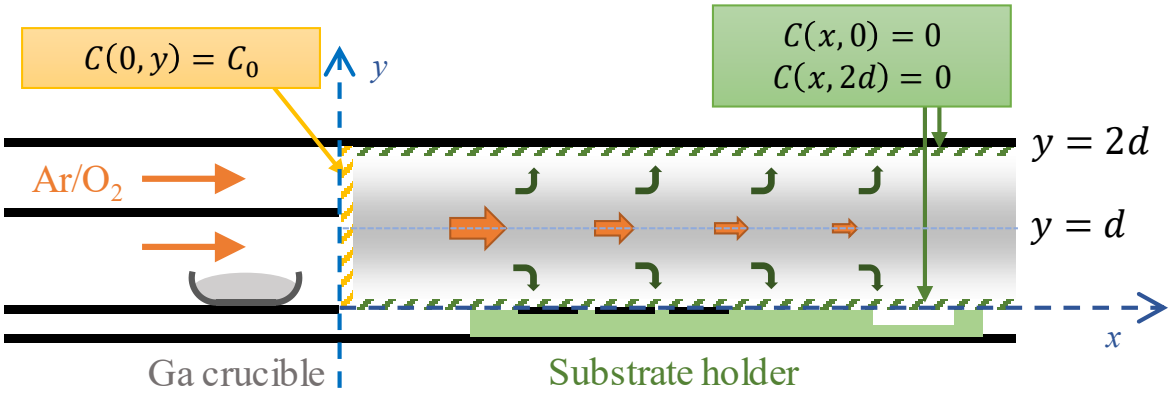
$C(0,y) = C_0$
y
$C(x,0) = 0$
$C(x,2d) = 0$
$y = 2d$
$y = d$
Ar/O_2
x
Ga crucible
Substrate holder

Figure 7

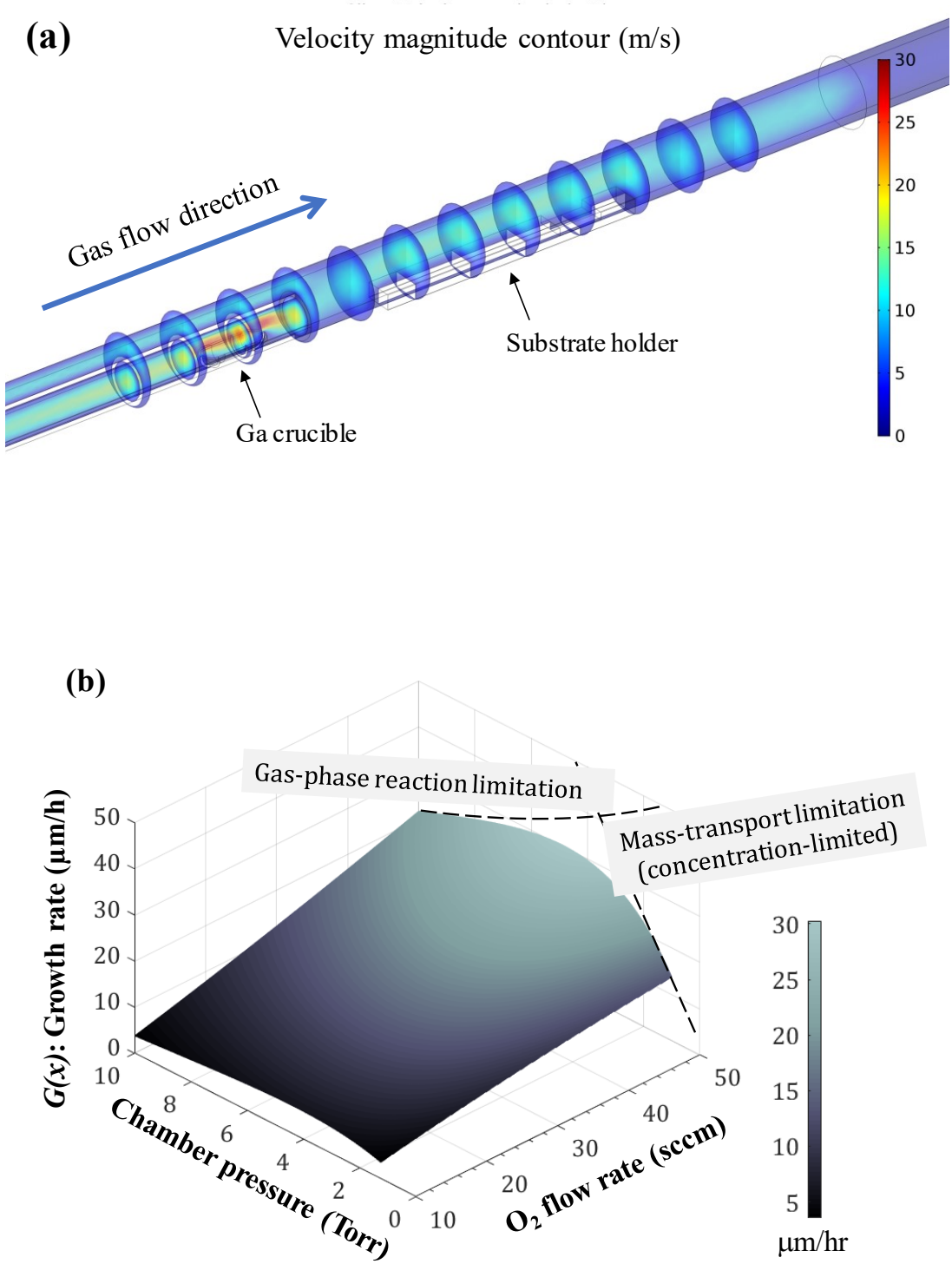
(a)
Velocity magnitude contour (m/s)
30
25
20
15
10
5
0
Gas flow direction
Substrate holder
Ga crucible
(b)
Gas-phase reaction limitation
Mass-transport limitation
(concentration-limited)
G(x): Growth rate (μm/h)
50
40
30
20
10
0
10
8
6
4
2
0
Chamber pressure (Torr)
10
20
30
40
50
O2 flow rate (sccm)
30
25
20
15
10
5
μm/hr